

International Conference on Space Optics—ICSO 2006

Noordwijk, Netherlands

27–30 June 2006

Edited by Errico Armandillo, Josiane Costeraste, and Nikos Karafolas



Towards a laboratory breadboard for PEGASE, the DARWIN pathfinder

F. Cassaing, J.-M. Le Duigou, B. Sorrente, B. Fleury, et al.



TOWARDS A LABORATORY BREADBOARD FOR PEGASE, THE DARWIN PATHFINDER

F. Cassaing¹, J.-M. Le Duigou², B. Sorrente¹, B. Fleury¹, N. Gorius², F. Brachet³, C. Buisset^{4,5}, M. Ollivier³, F. Hénault⁴, D. Mourard⁴, Y. Rabbia⁴, M. Delpech², P.-Y. Guidotti², A. Léger³, M. Barillot⁵, D. Rouan⁶, and G. Rousset^{6,1}

¹Office National d'Etudes et de Recherches Aérospatiales 29 av Div. Leclerc, BP 72, F-92322 Châtillon

²Centre National d'Etudes Spatiale, 18 av Edouard Belin, F-31401 Toulouse CEDEX 4

³Institut d'Astrophysique Spatiale, Bât 121, Univ Paris Sud, F-91405 Orsay

⁴Observatoire de la Côte d'Azur, BP 4229, F-06304 Nice CEDEX 4

⁵Alcatel Alenia Space, 100 Bd du Midi, BP 99, F-06156 Cannes La Bocca

⁶LESIA, Observatoire de Paris, 5 pl Jules Janssen, F-92195 Meudon

ABSTRACT

PEGASE, a spaceborne mission proposed to the CNES, is a 2-aperture interferometer for nulling and interferometric imaging. PEGASE is composed of 3 free-flying satellites (2 siderostats and 1 beam combiner) with baselines from 50 to 500 m. The goals of PEGASE are the spectroscopy of hot Jupiter (Pegasides) and brown dwarves, the exploration of the inner part of protoplanetary disks and the validation in real space conditions of nulling and visibility interferometry with formation flying.

During a phase-0 study performed in 2005 at CNES, ONERA and in the laboratories, the critical subsystems of the optical payload have been investigated and a preliminary system integration has been performed. These subsystems are mostly the broadband (2.5-5 μm) nuller and the cophasing system (visible) dedicated to the real-time control of the OPD/tip/tilt inside the payload. A laboratory breadboard of the payload is under definition and should be built in 2007.

Key words: Interferometry, Nulling interferometry, Cophasing, Formation flying.

1. CONTEXT

In 2004, CNES issued a call for scientific proposals for spaceborne formation flying missions. A consortium led by IAS and including other scientific laboratories and AAS, proposed the PEGASE mission [1]. It was selected to proceed through a phase 0 process in 2005 (fig. 1).

The PEGASE mission and a preliminary design from the work of phase 0 are described in details in a companion paper [2]. Although it is far less demanding than for the study of terrestrial exo-planets, the PEGASE payload is

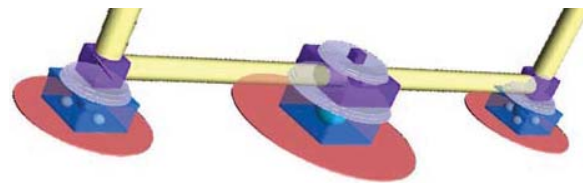


Figure 1. Simplified view of PEGASE.

just at the border of current state of the art and requires some complementary investigations. CNES has thus decided to support R&D programs, currently performed in parallel in the laboratories, to investigate in detail critical points of the payload. In addition, the consortium is currently defining and will build (upon CNES approval) a global laboratory breadboard for the payload.

The following section of this paper gives an overview of the PEGASE payload. In section 3, results from current R&D programs are presented. Specifications for the laboratory breadboard are listed in section 4, and a preliminary definition is given.

2. THE PEGASE PAYLOAD

The work performed at CNES during the phase 0 showed that formation control at the satellite level (star trackers, RF or optical metrology) is not sufficient for nulling. Therefore, the payload has to include a fine cophasing stage, using light from the observed object (or its bright parent star). We also have to cope with a limited volume (120 x 120 x 60 cm) because of the system choice to fit into a Soyuz fairing, without deployable sun shields. The reliability in space environment imposes the redundancy of all mechanisms. The number of components was minimised to reduce the complexity and maximise the optical transmission. Another guideline was to minimise the

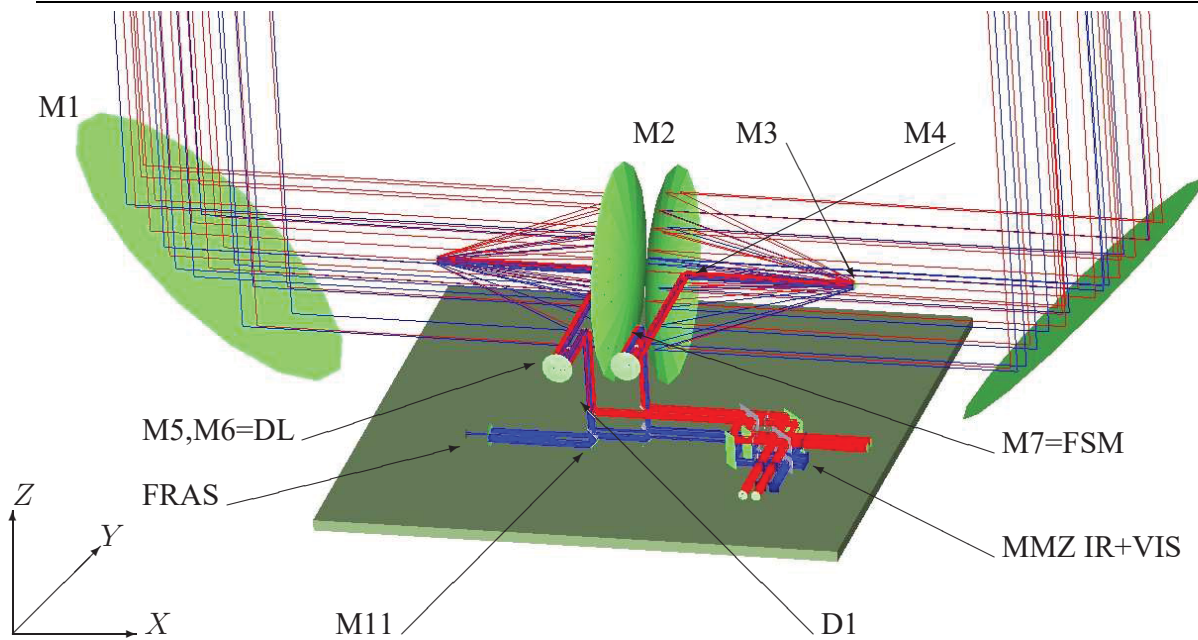


Figure 2. Preliminary optical layout.

coupling of various degrees of freedom, either at satellite level or in the payload itself. Last, the two arms of the interferometer shall have a maximum symmetry w.r.t. reflections to minimise the differential polarisation effects. A possible optical layout is illustrated in fig. 2.

The 3D layout gives a compact design and allows to implement the most critical parts, the nulling interferometer and the cophasing sensors on the same base plate.

Siderostats *M1* is a flat non-deployable mirror with 45° inclination and an elliptical aperture. It is the only part of the payload mounted on the small lateral spacecrafts. The size of *M1* (70 x 50 cm) is constrained by the relative positioning of the spacecrafts in the fairing.

Beam Compressor *M2* – *M3* form a simple afocal, with a magnification $G=20$ which defines the size of the beams (2 cm) in the payload. An off-axis afocal has also been considered, but this leads to a smaller collecting aperture and a larger optical bench assuming $f/D > 1$.

Achromatic phase shifter Because PEGASE is a two-beam nuller, a π phase shift is required between the two beams. Two main classes of Achromatic Phase Shifter (APS) can be considered. Geometric APS are based on a 180° field reversal by folding mirrors [3]. Dioptric APS are based on a combination of dielectric materials with different index/thickness, as used on the Synapse [4] or MAI2 [5] breadboards.

Because the two siderostat mirrors *M1* intrinsically provide the first stage of a geometric APS, and since another 45° reflection is required to extract after the beam compressors the two counter-propagating beams towards the active stage, the geometric APS has been chosen and its second stage is implemented with the small flat mirror *M4*. With this solution, the APS is also seen by the cophasing sensors and thus its drifts can be compensated.

However, the use of dispersive prisms to compensate for small chromatism effects is not excluded.

Active stage During the nulling measurement, there is no satellite actuation. Small drifts are corrected in the payload, by a Delay Line (DL) for Optical Path Difference (OPD) and by a Fine Steering Mirror (FSM) for tip/tilt. The DL is the *M5* – *M6* cat's eye, with a ± 1 cm stroke and 1 nm rms resolution typically, for example with magnetic bearings and voice coil actuation [6]. The FSM *M7* redirects the beams along $-Z$ to the combining stage. Each FSM uses three piezoelectric actuators with 15 μ m stroke and nanometric resolution, assuming a 100 V maximum voltage and a 5 mV electronic noise.

The stop is imposed on the FSM so that the tip/tilt correction does not affect the OPD. Placing the DL before the FSM ensures that the pupil does not move in the FSM-nuller space, and allows the pupil to be re-imaged backwards (thanks to the curvature of *M6*) near *M3*, to minimise the shift of the central obscuration with field.

Combining stage A dichroic plate *D1* transmits the wavelengths below 1.5 μ m and reflects higher wavelengths toward the fully symmetric and achromatic nuller. Because integrated optics is not yet mature in the PEGASE spectral band, whereas bulky optics has already been validated on ground, a Modified Mach-Zehnder (MMZ) has been preferred [7].

The four outputs of the MMZ are focused by small off-axis parabolas into single mode fibers used to get rid of the WFE errors of the two beams. They are made of fluoride glasses ($\lambda_c=2.5$ μ m, NA=0.15, $r_c=6.32$ μ m, ZrF₄ based glasses [8]).

Detection module The fibers are connected to a detection stage (not shown in fig. 2), including a dispersing prism and a HgCdTe based detection matrix. It will lie toward

the +Y side of the bench, with a high thermal decoupling and a link to a sufficient radiative area on the +Z face.

Internal loop sensors The visible (or more precisely $\lambda < 1 \mu\text{m}$) part of the spectrum is divided between the Fringe Sensor (FS) used for OPD control and the FRAS (Field Relative Angle Sensor) used for tip/tilt control. The exact allocation is still to be optimised. The FS is another MMZ with the four classical ABCD outputs [9] generated by a spatial modulation. Both MMZ are superimposed, so that differential drifts such as the ones detected in the recent nulling breadboards [4] are minimised. The FRAS is based on a Cassegrain small telescope with a classical 1024x1024 Si-based CCD, where 1 pixel represents 0.18 arcsec on the sky. Each beam uses a different 512x512 sub-matrix thanks to a small differential tilt angle of the M11 mirrors. The estimated resolution of the camera is 10 mas.

Calibration system The payload will also include internal sources and injection devices for on-ground alignment and tests, and in-flight calibration purpose. These systems are not represented in fig. 2.

Other devices The +Y part of the bench will be used to implement metrology sensors required by the formation control [2], a precise star tracker (1 arcsec) and possibly a laser metrology system that could be of the Mouse type [10]. Electronics will be located outside the optical bench, in the service module, to avoid thermal sources.

3. CURRENT R&D RESULTS

This section describes on-going R&D activities in the laboratories of the PEGASE consortium. Nulling is investigated at IAS with the SYNAPSE bench [4] and at AAS with the MAI2 bench [5]. Cophasing is investigated at ONERA, by simulation or with the BRISE bench [11].

3.1. The nuller

Tests performed at AAS investigate polarisation effects as detailed in a dedicated paper [12]. Tests were carried out with polychromatic beams ($\lambda_0=1.55 \mu\text{m}$ and $\Delta\lambda/\lambda=5\%$). With both polarisations and over an interval of several tens of seconds, the average value of the nulling is : $\langle N \rangle = 3 \cdot 10^{-5}$ and the standard deviation is : $\sigma_N = 6 \cdot 10^{-6}$. The best recorded nulling is : $\langle N \rangle = 2.7 \cdot 10^{-5}$. With only one polarisation, the average value of the nulling is $\langle N \rangle = 9 \cdot 10^{-6}$ and the standard deviation is $\sigma_N = 5 \cdot 10^{-7}$. The best recorded nulling is $\langle N \rangle = 6 \cdot 10^{-6}$.

Tests performed at IAS focus on the stability issue. Measurements have been made on the SYNAPSE test-bed in the K band, between 2 and 2.5 μm . Fig. 3 shows the best result obtained so far, with a stellar leakage level near $1.5 \cdot 10^{-4}$ (or a rejection ratio of 6 500) and maintained during several minutes. This graph represents the temporal

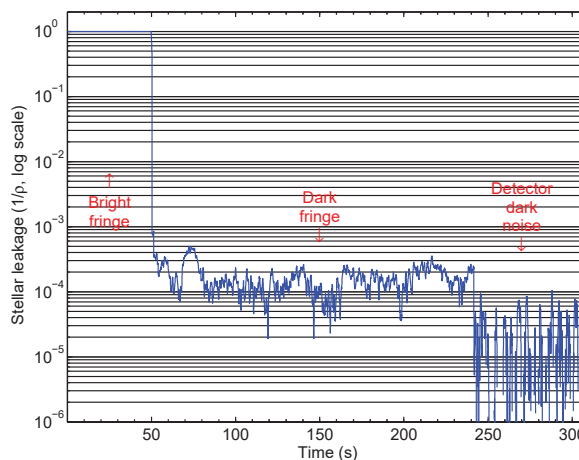


Figure 3. Stellar leakage variations with time.

interferometric signal recorded on one of the two destructive beams, after the modal filtering provided by a single mode fiber. The transition between the bright ($0 < \text{time} < 50 \text{ s}$) and the dark ($50 < \text{time} < 240 \text{ s}$) fringes is due to a volunteer variation of the OPD, by means of a delay line. The dark current noise ($240 < \text{time} < 310 \text{ s}$) was then recorded with a mirror placed in front of the detector. Finally, these measurements have been made without any OPD correction while recording.

Though encouraging, further measurements have shown the existence of stellar leakage drifts if no correction is made on the OPD. A closed-loop control of the OPD, based on the data provided by a metrology channel superimposed on the scientific beams, did not correct these drifts and even tend to amplify them. One reason could be the distance between the metrology and the scientific beams, close to 20 mm.

To solve this problem, a technique based on OPD modulation has been implemented. The idea is to compare the two stellar leakage signals measured for two small OPD near the supposed dark fringe minimum. An error signal is then deduced and used to correct the OPD to tend towards this minimum. Fig. 4 shows another stellar leakage measurement, recorded with OPD modulation, with 5 nm OPD steps. The stellar leakage level is $3.8 \cdot 10^{-4}$ and it shows the possibility to maintain this level during periods longer than six hours.

This method is currently under test, but first results tend to show it could be a very promising, though time consuming, technique to reach the stability required during the integration times needed to characterise exoplanets.

3.2. The star tracker

The performance of the tip/tilt loop is evaluated at ONERA. Starting with the satellite residual pointing, the fine pointing loop has to ensure a symmetrical coupling into

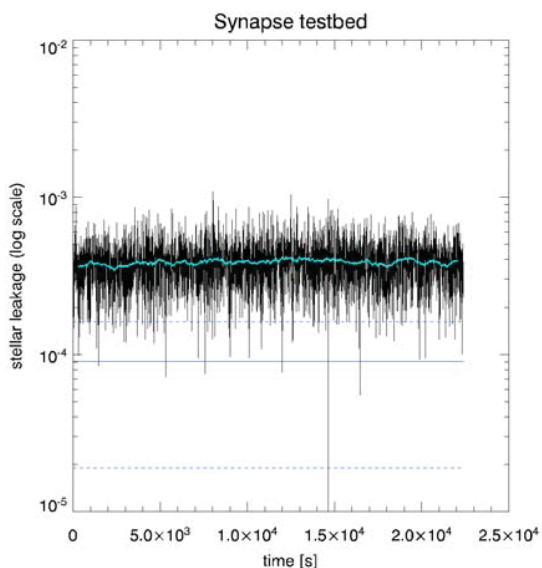


Figure 4. Stellar leakage variations with time, with OPD modulation. This graph represents the temporal interferometric signal of the dark fringe. The OPD is corrected at a frequency of 0.16 Hz, during more than six hours. The mean dark current value is represented by the continuous horizontal line on the bottom of the graph, while the dotted lines correspond to its standard deviation. A sliding average of the signal, based on ten minutes, has been superimposed to the raw data.

the fiber (intensity mismatch smaller than 1% with 0.3% rms fluctuations) and a minimal loss of flux (transmission > 0.7 from 2.5 to 5 μm). The focal length of the injection parabola is adjusted to optimise the coupling at 2.5 μm . Assuming the Strehl approximation for calculating the coupling efficiency [13], this leads to a specification of around 30 mas per axis for the pointing accuracy.

Since the FSM are located after the beam compressors M2-M3, their magnification G impacts on the dynamics of the tip-tilt errors (dynamical disturbances and drift effects due to various sources like alignment errors, thermal dilatation or gravity release), noise and stroke actuation and mechanical constraints. The current trade-off is $G=20$ and an angular stroke of ± 65 arcsec for the FSM, including a 35% cut off for operation at 100 K. The first estimates of differential polarisation effects induced by the $45^\circ \pm 65$ arcsec angle show that the impact on nulling performance is less than 10^{-8} . Regular calibration procedures are foreseen to maximise the coupling efficiency into the fibers and to measure the interaction matrix between the FSM voltages and the spot position in the camera plane.

The exposure time required to reach a 10 mas contribution for the photon noise has been computed for the target stars. Fig. 5 plots the estimated exposure time versus the wavelength assuming a spectral bandwidth $\Delta\lambda/\lambda= 2.5$ and a total transmission of 0.11 in the considered spectral

domain. It appears that the exposure time can be smaller than a few ms for most of the stars which means that the contribution of the photon noise is not dominant. The main task should be to correct the disturbances due to instrumental vibrations and control attitude errors. Fig. 5 also shows that the best spectral domain for the FRAS is the visible-near infrared, where the stellar spectrum reaches its maximal values for most stars.

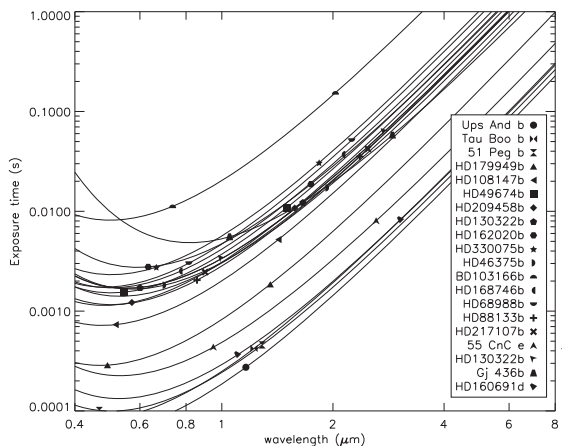


Figure 5. Fine pointing integration time vs wavelength.

These results will be improved in 2006, using an optimised algorithm to minimise the contribution of photon noise. In addition, a representative tip/tilt loop will be implemented on BRISE for experimental tests.

3.3. The fringe tracker

Performance of the OPD loop is also evaluated at ONERA. In the observing mode, the main requirement is that the residual OPD should be less than 2.5 nm rms. The exact performance can not be estimated for the moment, since the amplitude of most disturbances is not known at the nanometer level. What can be done is to suppose that the FS and the DL are run at the maximum frequency to sufficiently damp all the OPD contributors, so that the residual OPD comes mostly from the measurement noise of the FS and is equal to 2.5 nm rms. Since the FS noise is directly linked to the number of detected photons [14] and since the magnitude of all the targets is known, an estimate of the FS integration time can be derived as plotted in fig. 6. An integration time of about 20 ms is sufficient for most targets, i. e. a correction frequency from around 50 Hz up to 200 Hz for a few targets. This should be sufficient to control OPD contributors at low frequency (residual speed, differential solar pressure,...) or at high frequency (micro-vibrations) since their amplitude is smaller and advanced control techniques (such as Kalman filtering) can be used for known disturbances (constant acceleration, sinusoidal harmonics). This figure also shows that the best spectral domain for the FS is below 1.5 μm , and can be covered efficiently by silicon

detectors. To optimise the measurement, a rather large spectral band ($\Delta\lambda/\lambda=2.5$) and a small number of pixels (photon-noise regime) have been assumed.

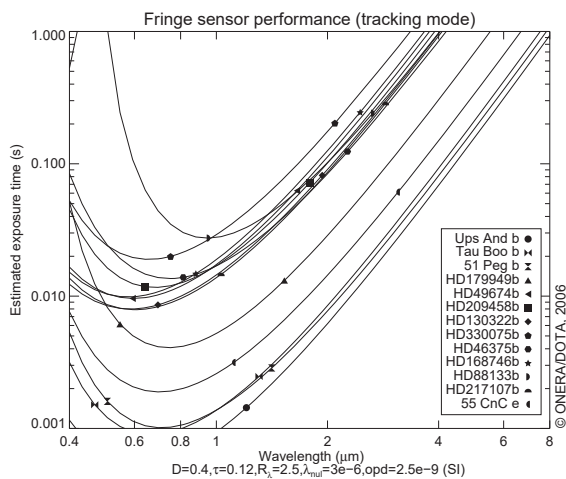


Figure 6. Estimation of the integration time required in the FS to reach an OPD accuracy of 2.5 nm.

In the acquisition mode, the OPD between the beams can be much larger than the coherence length of the FS. It is thus necessary to perform a fringe search, by moving the DL or waiting for the fringes to pass while the satellites drift. Because of the hectometric baseline, the speed v of the fringes can reach several hundreds of $\mu\text{m/s}$. To avoid blurring, the exposure time T_p of the FS must therefore be close to 1 ms, and the repetition time T_r small enough so that measurements at locations vT_r correctly sample (N_v times) the chromatic envelope of the fringe pattern, which coherence length is given by the number of spectral channels N_λ . Fig. 7 shows that for detection, the best spectral domain is shifted towards the IR, because the long wavelengths suffer less blurring. However, for the targets of interest, a SNR larger than 10 is possible with a silicon detector with realistic parameters for the real-time processor and an external OPD drift up to 200 $\mu\text{m/s}$.

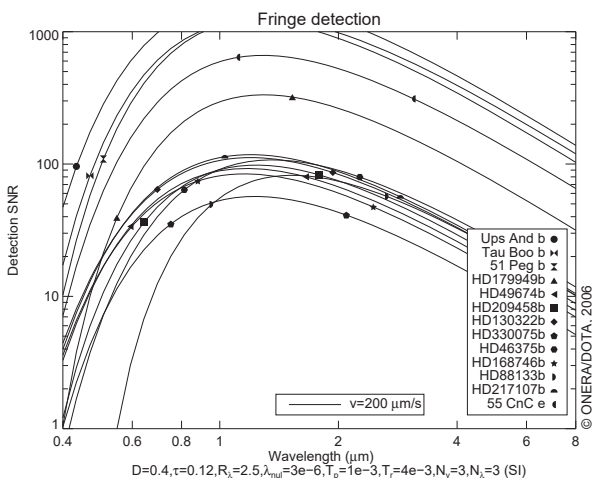


Figure 7. Fringe detection SNR in the acquisition mode.

The FS must meet requirements from the acquisition and tracking modes. In order to reach the kHz sampling rate with a minimum number of pixels, a coaxial beam combiner is the most relevant to combine the two beams. To cope with stability requirements and the fast fringe drift, a spatial modulation is used without any moving part. Such a FS has already been investigated in our team for stellar interferometry on ground [15]. Light from each of the four $\pi/2$ phase-shifted outputs is dispersed and focused on a linear array of pixels. Using all the available visible range (between 0.6 and 0.9 μm , cut in 3 spectral channels of 100 nm) gives a spectral resolution $R_\lambda=2.5$.

The OPD loop will also be validated on the BRISE bench.

4. THE PEGASE LABORATORY BREADBOARD

In addition to the previously described sub-system activities, it has been decided in 2005 between CNES and the PEGASE consortium to include in the R&D effort the development of a laboratory breadboard of the payload. This breadboard will be defined in 2006, and upon CNES approval by the end of 2006, it will be built and operated inside the consortium.

4.1. Goals of the breadboard

The goal of the breadboard is to demonstrate the feasibility of the PEGASE optical payload, by merging a nulling interferometer and OPD/tip/tilt control loops. Main focus will be put on the following points:

1. Obtain an average null of 10^{-4} with a 10^{-5} stability over a few hours in several spectral bands between 1.5 μm and 5 μm .
2. Validate fringe acquisition with a drift speed up to 150 $\mu\text{m/s}$.
3. Characterise the noise and the maximum external drift allowed for the two active loops (OPD and tip/tilt).
4. Investigate interaction between the OPD/tip-tilt/flux loops.
5. Investigate the calibration procedures, taking into account measurements from the cophasing loops. Calibration can be performed before the nulling measurement (estimation and correction of non-common path aberrations) or after the nulling measurement (estimation of the leakage from perturbation residuals measured by the real-time sensors).
6. Demonstrate the differential stability between the nulling and cophasing sensors.
7. Validate the full operation with realistic external disturbances (star/fringe acquisition, tracking, unloading of small-stroke fine correctors).

4.2. Preliminary design

The specification and design of the breadboard is currently under way. Its main components will probably be:

- The source simulator, in the VIS+IR spectral bands.
- The most critical sub-systems: the nuller + IR detector and the two cophasing sensors (FS and FRAS), with minimum differential paths.
- The fine-stage correction system, that will most probably be based on small-stroke PZT piston/tip/tilt stages, that will also be used in a first step to introduce perturbations.
- A representative optical train to introduce 3D effects (polarisation) and coatings (VIS+IR).
- A simulator of real perturbations computed from a free-flying flight model (long stroke delay-line, pseudo-siderostats to introduce combined piston/tip/tilt errors).

5. CONCLUSION

The work performed during the phase 0 study shows that the PEGASE mission can be based on a rather simple design of the payload, such as the one presented here. PEGASE is thus an intermediate (necessary ?) path-finder mission on the road leading to the direct observation of Terrestrial exo-planets with free-flying nullers. Although some major trade-offs are still open and remain to be investigated in more details during a future phase A, work is currently in progress in several laboratories to demonstrate the feasibility of the most critical sub-systems, with encouraging results.

The PEGASE laboratory breadboard is intended to demonstrate a wide-band nulling in presence of realistic phase disturbance, corrected by a cophasing system fed by light from the target star itself. It will be built in 2007 upon CNES approval and should give its first results in 2008. Such a bench will be a major step in the feasibility demonstration of future free-flying interferometers.

REFERENCES

1. X. Leyre, E. Thomas, M. Barillot et al. First formation flying interferometer demonstrator mission including on flight Bracewell nulling. In *2nd international symposium on formation flying missions and technologies*. American Institute of Aeronautics and Astronautics, 2004.
2. J.-M. Le Duigou, M. Ollivier, F. Cassaing et al. Pegase : a formation flying interferometer for the spectroscopy of giant exo-planets. In *Sixth International Conference on Space Optics* [16].
3. E. Serabyn, J. K. Wallace, G. J. Hardy et al. Deep Nulling of Visible Laser Light. *Appl. Opt.*, 38:7128–7132, December 1999.
4. F. Brachet. *Etude et developpement d'un déphaseur achromatique pour l'interférométrie en frange noire*. PhD thesis, Université Paris-Sud (XI), 2005.
5. V. Weber, M. Barillot, et al. Nulling interferometer based on an integrated optics combiner. In *Astronomical Telescopes and Instrumentation*. Proc. Soc. Photo-Opt. Instrum. Eng., 2004.
6. T. van den Dool, F. Kamphues, B. Fouss et al. The design of a breadboard cryogenic optical delay line for DARWIN. In Alan F. M. Moorwood and M. Iye, editors, *Ground-based Instrumentation for Astronomy*, volume 5495, pages 39–50. Proc. Soc. Photo-Opt. Instrum. Eng., September 2004.
7. E. Serabyn and M. M. Colavita. Fully Symmetric Nulling Beam Combiners. *Appl. Opt.*, 40(10):1668–1671, April 2001.
8. G. Mazé et al. Fluorid glass fibers for light transmission up to 5 μm . In *Astronomical Telescopes and Instrumentation*, volume 484, pages 93–98. Proc. Soc. Photo-Opt. Instrum. Eng., 1984.
9. M. Shao, M. M. Colavita, B. E. Hines et al. The Mark III Stellar Interferometer. *Astron. Astrophys.*, 193:357–371, March 1988.
10. J.M. Le Duigou and A. Poupinet. The MOUSE II sensors for longitudinal measurements. In *Proceedings of the OPTRO 2005 International Symposium*, Paris, France, 2005. AAAF.
11. F. Cassaing, B. Sorrente, L. Mugnier et al. Brise: a multipurpose bench for cophasing sensors. In J. D. Monnier and M. Schöller, editors, *Advances in stellar interferometry*, volume 6268. Proc. Soc. Photo-Opt. Instrum. Eng., 2006.
12. C. Buisset. Multi-axial nulling interferometry: Demonstration of deep nulling and investigations of polarization effects. In *Sixth International Conference on Space Optics* [16].
13. C. Ruilier and F. Cassaing. Coupling of large telescopes and single-mode waveguides: application to stellar interferometry. *J. Opt. Soc. Am. A*, 18(1):143–149, January 2001.
14. F. Cassaing. Optical path difference sensors. *C. R. Acad. Sci. Paris*, Série IV, tome 2(1):87–98, January 2001.
15. F. Cassaing, B. Fleury, C. Coudrain et al. An optimized fringe tracker for the VLTI/PRIMA instrument. In P. J. Léna and A. Quirrenbach, editors, *Interferometry in optical astronomy*, volume 4006, pages 152–163, Bellingham, Washington, 2000. Proc. Soc. Photo-Opt. Instrum. Eng., SPIE.
16. *Sixth International Conference on Space Optics*, 2006.